Echavarria, AM.; Rico Tortosa, PM.; Gómez Ribelles, JL.; Pacha-Olivenza, MA.; Fernandez-Calderon, M.; Bejarano-G, G. (2017). Development of a Ta/TaN/TaNx(Ag)y/TaN nanocomposite coating system and bio-response study for biomedical applications. Vacuum. 145:55-67. doi:10.1016/j.vacuum.2017.08.020

Development of a Ta/TaN/TaNx(Ag)y/TaN nanocomposite coating system and Bio-response study for biomedical applications

*Aida M. Echavarría[1], P. Rico [2,3], J. L. Gómez Ribelles[2,3], Miguel A. Pacha-Olivenza [4,5], María-Coronada Fernández-Calderón[5,6], Gilberto Bejarano G[*1].*

[1] Centro de Investigación, Innovación y Desarrollo de Materiales – CIDEMAT, Facultad de Ingeniería, Universidad de Antioquia, Medellín, Colombia

[2] Center for Biomaterials and Tissue Engineering, CBIT, Universitat Politècnica de València, Spain

[3] Biomedical Research Networking Center in Bioengineering, Biomaterials and Nanomedicine (CIBER-BBN), Valencia, Spain

[4] Departamento de Física Aplicada, Facultad de Ciencias, Universidad de Extremadura, Badajoz, Spain

[5] Centro de Investigación Biomédica en Red en Bioingeniería, Biomateriales y Nanomedicina CIBER-BBN, Badajoz, Spain

[6] Departamento de Microbiología, Facultad de Medicina, Universidad de Extremadura, Badajoz, Spain

*E-mail: gilberto.bejarano@udea.edu.co

Abstract

TaN(Ag) composited coatings are being investigated to improve biocompatibility of different biomedical devices due to the mechanical and chemical stability of TaN and bactericidal effect of silver nanoparticles. However, controlling the size, density, shape and especially the release of silver ions (Ag) into the surrounding medium becomes a challenge, since elevated levels of Ag could be cytotoxic. The aim of this work is to design and develop a new Ta/TaN/TaNx(Ag)y/TaN coating system, deposited by unbalanced DC magnetron sputtering technique, presenting an adequate balance between biocompatibility and bactericidal effect for potential applications in biomedical field. For this purpose, four different coating systems were deposited on 316L stainless steel and silicon (100) samples applying a bias voltage of -30, -60, -90 and -120V during the deposition of the top layer of TaN to vary its density. This manufacturing strategy allowed controlling the diffusion of silver nanoparticles to the coating surface and the release kinetics of silver ions in simulated body fluid (SBF). Biologic characterization has been performed with MC3T3-E1 pre-osteoblastic cells in terms of cell adhesion and long-term differentiation. Additionally, the adhesion and biofilm formation of the bacteria *Streptococcus sanguinis* strain in the deposited coating systems of Ta/TaN/TaNx(Ag)y/TaN were analyzed. The results indicated an improvement of cell adhesion and differentiation of the composited coating deposited with a bias of -30V compared to other coatings. Concordantly, this coating showed the lowest bacterial adhesion and biofilm formation, representing an attractive and suitable composited material for biomedical applications.

KEYWORDS: biocompatible coatings, Ag nanoparticles, biomedical devices, magnetron sputtering, MC3T3 preosteoblastic cells, *Streptococcus sanguinis*.

1. Introduction

In the recent decades, numerous studies have reported diverse surface modification techniques for metallic materials such as AISI 316L stainless steel and titanium alloys, widely used in the manufacture of implants for bone tissue and divers biomedical devices like a surgical instrumentation. Many strategies have been employed (1,2) for surface bio-functionalization, in order to obtain roughness values, nanostructured patterns, metallic inclusions, and anchorage of organic molecules (1,2).The ultimate aim of these surface modification is to favor cell adhesion, increase gene expression and differentiation of osteoblasts (3), and consequently to achieve the rapid regeneration of bone tissue from a successful osseointegration process. The formation of duplex coatings by means of the diffusion of nitrogen in the steel surface makes it possible to control the precipitation of nitrate, preserving corrosion and wear resistance caused by free chromium matrix (4,5).

Tantalum element (Ta) is in the focus of biomedical research, due to its known non-toxic behavior, on account of its high chemical and thermal stability, which prevents adverse reactions or body alterations (6–8).The invention of the tantalum porous foam on Ti6Al4V alloy substrates used in the advancement of orthopedic applications (9) is an illustration of this phenomenon. Recently, tantalum nitride (TaN) has been developed through different methods including RF magnetron sputtering (PVD) (10), chemical vapor deposition (CVD) by thermal controlled process with a precursor of Ta foams (11,12), or atomic layer deposition (PEALD) in a NH_3 rich plasma (13).

Although TaN coating has been little explored in the literature, there are some works that focus on characterizing mechanical and tribological properties of its structure (14,15) describing it as an hard and high wear resistance coating (16,17). Some reports described its particular electrical properties that allow vast utility as resistors in integrated circuits (18–20). Among the many applications intended for this coating in the field of biomedicine, the most promising could be its application in orthopedic prosthesis in order to further improve the interaction process between the device and bone tissue (21). However, to date industrial application of this kind of coatings is at an early stage (22).

Bacterial adhesion and subsequent biofilm formation on the surface of implantable biomaterials are an important focus of pathogenesis infection (23). Metallic inclusions of metal nanoparticles that act as broad spectrum bactericide elements such as silver (Ag) (24–26) in coatings formed by a ceramic matrix such as TaN, could effectively counteract the anchoring and bacteria colonization of metallic biomaterials in bone implantation. Nevertheless, precise control of the delivery of the nanoparticles is essential in order not to affect cell viability levels (27–30). Multilayer duplex coating systems of TaN(Ag) that include layers containing silver nanoparticles - Ag(NPS) - and layers controlling their diffusion, make possible to improve both mechanical and antimicrobial performance of susbtrates.

Cytotoxicity and bacterial effectiveness of Ag(NPS) are related to its amount or concentration in coatings, as well as its strong surface oxidation and its capability to release ions in biological media (31,32). The size of the nanoparticles also plays an important role in the biological response. This shows that the smaller the particle, the larger the surface area, hence the dissolution rate and reaction in aqueous medium increases (33–35).Diseases such as peri-implantitis and peri-implant mucositis, which result from biofilm formation and bacterial colonization, cause implant loss due to degeneration of connective tissue and mucosal destruction leading to possible bone resorption and disengagement of the implant (36,37) in the case of oral applications. *Duske et*. al reported that in a period of 10 years near 10% of implants placed were affected by advanced peri-implant mucositis (38), while other authors indicated that around 20% developed peri-implantitis after surgical procedures (39,40).

The aim of this work was the design and development of a Ta/TaNx(Ag)y/TaN coating system (hereinafter named TaNx(Ag)y) deposited by unbalanced DC magnetron sputtering technique, presenting an adequate balance between biocompatibility and bactericidal effect. In order to control the diffusion of silver to the surface of the coatings, a TaN diffusion layer was deposited by varying the bias voltage during the deposition; This provides a greater degree of densification in the surface structure of the coating acting as a barrier. Biocompatibility of the systems has been evaluated in terms of cell adhesion, cell morphology, long term growth and functional differentiation of murine MC3T3-E1 pre-osteoblastic cells. In addition, we analyzed the behavior of the different materials in relation to initial adhesion and biofilm formation of the bacterial strain *Streptococcus sanguinis*. Streptococcus have been selected as they constitute 20 % of all supragingival microorganisms present in the oral microbiota(41) and 80% of the settlers during the first phase of biofilm formation(42).

2. Materials and methods

2.1 Substrate preparation

316L stainless steel substrates (19 mm in diameter and 3 mm thickness) and single crystalline silicon (111), were coated with a duplex coating system consisting of pulsed plasma nitriding and subsequent deposition of a TaN coating. A rectangular self-manufactured vacuum chamber with dimensions of 700 x 700 x 800 mm^3 was used and the unbalanced DC magnetron sputtering technique was applied. All steel samples were polished using SiC emery paper with a grain size between 300 and 1200 and subsequently polished in alumina aqueous solution to a mirror finish until an average roughness of Ra= 0.05μm was obtained. The polished samples were cleaned in an ultrasonic bath with alcohol-acetone solution for 15 minutes. Before nitriding, all substrates were subjected to ionic cleaning for 30 minutes in Ar/H_2 plasma at a pressure of 31 Pa, temperature of 120 °C and bias voltage of -430 V. Nitriding of the samples was carried out for 7 hours at 350 °C, pulsed bias voltage of -750 V (on 80 μs and off 20 μs), keeping constant pressure and using an $Ar /N_2/H_2$ atmosphere with a gas flow ratio of 18:15:15 sccm, respectively. The low temperature of plasma nitriding was used to avoid the precipitation of chromium carbides, conserving the corrosion resistance of 316L steel.

For the manufacture of the coatings, two rectangular targets located opposite each other of Ta and Ag with a purity of 99.5 % and dimensions of 100 x 100 x 500 mm^3 were used. Before the composite coatings of TaNx(Ag)y were deposited, an ionic cleaning of substrates was performed for 30 minutes in a gas mixture of H_2/Ar at a pressure of 8 Pa, substrate bias voltage of -650 V (on 80 μs and off 30 μs) and a temperature of 120 °C.

2.2 Development of a Ta/TaN/TaNx(Ag)y/TaN nanocomposite coating

Ta and TaN adhesion layers with a total thickness of around 120 nm were deposited first on the sample surface as shown in Figure 1. The adhesion layers reduce the residual stresses caused by the differences of the crystalline structures and nature of the substrate (metallic) and the coating (ceramic). Moreover, this first layer (adhesion layer) improves the adhesion of the subsequent layers and reduces the porosity of the interface, whereby the corrosion process of the substrate could be delayed (43–46).The parameters used for the deposition of TaNx(Ag)y coatings like a silver reserve and for the upper diffusion layer of TaN are reported in Table 1.

After depositions of coatings, a set of the samples were subjected to heat treatment at 200° C for 4 minutes to promote the diffusion of Ag through grain boundaries to the surface. This heat treatment was carried out in a Nabertherm Brand oven with controlled nitrogen atmosphere. The heat treated samples were removed from the oven and immediately cooled with compressed air. The inclusion of the top diffusion layer of TaN (around 60nm in thickness) deposited at different bias voltages was aimed to act as a diffusion barrier for the silver particles in order to control their final size and release rate to the external environment.

Tantalum nitride doped with silver nanoparticles TaNx(Ag)y was deposited during 2 h and 40 min, applying a DC power of 1000 W and 70 W to the Ta and Ag target, respectively. All used process parameter are described in Table 1.

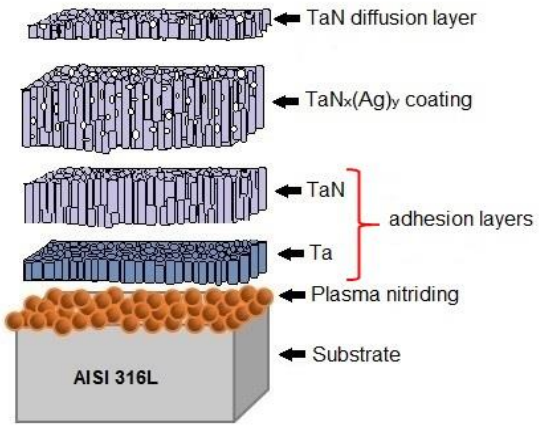

Figure 1. Design of $TaN_x(Ag)_y$ multilayer coatings deposited on plasma nitrided AISI 316L stainless steel.

Finally, a diffusion top layer of TaN was deposited on each TaNx(Ag)y coating applying a bias voltage between -30 and -120 V as consigned in Table 1. All coatings were deposited at a temperature of 273 °C, and substrates located at a distance of around 80mm from the targets and rotating at a speed of 30 rpm.

Table 1. Deposition conditions of TaNx(Ag)y multilayer coatings.

Pressure (mbar)	*$3{,}5x10^{-3}$*	
Bias voltage	*-70*	
Power Ta target (W)	*1000*	
Time coating (h)	*3*	
Sample $TaN_x(Ag)_y$	*Diffusion layer TaN Bias voltage (V)*	*Deposition rate (µm/h)*
30V-DL	*-30*	*0.327*
60V-DL	*-60*	*0.346*
90V-DL	*-90*	*0.344*
120V-DL	*-120*	*0.345*

2.3 Coatings characterization

Coatings morphology and topography were examined by scanning electron microscopy (SEM) with a JEOL JSM-6490LV device. The chemical composition of independent coatings was estimated by energy dispersive spectroscopy X-ray (EDX) operating at 15 KeV coupled to SEM and supported by INCA Energy software. Phases compositions were established with a X-ray diffractometer (Panalytical Empyream), using Cu Kα1 radiation with λ=1.540598 Å, 45 kV, 40 mA, incidence angle of 1° and step to 0.05° per second. In order to study the transversal morphology and distribution of layers in the coatings, thickness was assessed on the coatings obtained on silicon using a scanning electron microscope with a focused ion gun (FIB) incorporating a X-MaxN device, with a milling current of 50 pA and a voltage of 30 KV.

Ag released of the coated samples to the surrounding medium was detected by measuring in triplicate the Ag concentration in simulated body fluid (SBF) by Standard Method 3000 Metals (3030B preliminary treatment of samples b. filtration for dissolved and suspended metals), with a microwave-induced plasma atomic emission spectrometer, model MP-AES 4100, Agilent. After immersion of tests for 1, 8, 20 and 30 days. Substrates and coatings roughness (Ra) were obtained from 10 measurements with a Bruker Pektakxt contact profilometer with contact force of 3 mg for 30 s and a sliding distance of 1500 µm, in accordance with the DIN EN ISO 4287:1998 norm. The coatings and substrate micro hardness was evaluated through the nanoindentation method in an IBIS Authority Fischer – Cripps device, with a Berkovich diamond tip at 21 °C. The loading and unloading force was maintained at 0.026 mN/ nm at peak load of 3.5 mN; more than seven indentations were performed in a depth range of 80 to 120 nm (about 10% of the thickness of the coatings). The Oliver-Pharr method (47) was applied to determine the hardness (H). Structural properties such as, roughness, grain size, and tribological features like as coefficient of friction and wear rate of the different coatings can be consulted in previous published works (48,49).

Wettability tests for the coated and uncoated AISI 316L stainless steel substrate and contact angles were determined using 3 µL drops and utilizing three reference liquids: ultrapure water (Milli-Q) (polar liquid), formamide (polar liquid, Sigma) and glycerol (nonpolar liquid, Sigma) with known surface energy components (50,51). The surface free energy was determined using the Owens-Wendt-Rabel-Kaelble (OWRK) approach method (52,53).

2.4 Biocompatibilty evaluation of the coatings

The different coatings produced on steel samples were used as substrates of 19 mm diameter for cell cultures. Polished and unpolished AISI 316L stainless steel substrates were used as control. All samples were UV sterilized in a laminar flow cabinet for 1 hour prior to cell and bacterial seeding.

2.4.1 Pre-osteoblast cell culture

Commercial MC3T3-E1 preosteoblast cell line (RIKEN cell bank, Japan) was cultured in Dulbecco's Modified Eagle Medium (DMEM, Invitrogen) supplemented with 10 % fetal bovine serum (FBS, Invitrogen) and 1 % penicillin–streptomycin (P/S, Lonza). Cells were maintained in a humidified atmosphere at 37 °C and 5 % CO_2 and passaged twice a week using standard techniques avoiding cell confluence. In all experiments density of seeding was 10,000 cells/cm2. Each experiment was performed in triplicate.

2.4.2 Cell adhesion

To examine initial cell adhesion, cells were cultured for 3 h in DMEM (Gibco) supplemented with 10% FBS (Invitrogen) and 1% P/S (Lonza). After culture, cells were washed in Dulbecco´s phosphate buffered saline (DPBS, Invitrogen) and fixed in formalin solution (Sigma) at 4 ºC for 1 h. Samples were then rinsed with DPBS and permeabilized with DPBS / Triton x-100, 0.5 % for 10 min at room temperature (RT). To reduce background signal, samples were incubated in blocking solution (DPBS / Triton x-100, 0.1 % / goat serum 5 %) for 1 h and subsequently incubated in primary antibody anti-vinculin (Sigma) diluted 1:400 in blocking buffer for 1 h at 37 ºC. After that, they were washed in washing buffer (DPBS + Triton x-100, 0.1 %) 3 times for 5 min each, followed by incubation with labelled secondary antibody Cy3 (Santa Cruz Technologies) and BODIPY FL phallacidin (Invitrogen), diluted 1:200 and 1:400 respectively in blocking buffer for 1 h at 37 ºC for cytoskeleton staining. Finally, the samples were rinsed in washing buffer 3 times for 5 min each, and mounted in Vectashield containing DAPI staining (Vector laboratories). Samples were observed under an epifluorescence microscope (Nikon Eclipse 80i).

2.4.3 Cell differentiation

After 48 h of cell culture in basal medium (DMEM / FBS 10 % / P/S 1 %) allowing the cells to reach confluence, the cells were stimulated to differentiate with osteogenic differentiation medium (DMEM / FBS 10 % / P/S 1 % / Ascorbic Acid 50 µg/mL / β-glicerophosphate 10 mM / dexamethasone 0.1 µM). Osteogenic markers were evaluated after 15 days of culture. Immunostaining procedures were performed as explained above in section 2.4.2, but using the different antibodies indicated in Table 2.

Table 2. Primary and secondary antibodies used in differentiation experiments.

Osteogenic differentiation	*Primary antibody*	*Secondary antibody*
OPN	OPN mouse anti mouse, Santa Cruz Biotechnology, dilution 1:200	Alexa Fluor 488 goat anti mouse, Life Technologies, dilution 1:200
IBSP	IBSP rabbit anti mouse, dilution 1:200	Alexa Fluor 488 goat anti rabbit, Life Technologies, dilution 1:200

2.5 Bactericidal tests

2.5.1 Bacterial strain and culture

The oral bacterial strain used for adhesion and biofilm assays was *Streptococcus sanguinis* (ATCC 10556), obtained from the Spanish Type Culture Collection (CECT). The bacterial strain was routinely maintained in Brain Heart Infusion (BHI) (OXOID LTDA, Basingstoke, Hampshire, UK) agar or broth at 37 °C in 5 % CO_2 (Galaxy 170S, Eppendorf AG, Hamburg, Deutschland) to obtain cultures. These cultures were incubated in BHI broth with CO_2 atmosphere (5 %) for 18-24 hours at 37 °C. The times and volumes of the medium employed were in accordance with the feasibility and optimal growth conditions to carry out adhesion experiments of microorganisms, which were selected after analyzing the growth curve of the strain used.

2.5.2 Bacterial adhesion on the surface of the coatings

For the initial adhesion assay, the bacteria were then harvested by centrifugation for 5 min at 1000 g (Sorval TC6, Dulon, USA) and washed three times with phosphate buffered saline (PBS, pH 7.2) preconditioned at 37 °C. The bacteria were then suspended in PBS at a concentration of $3x10^8$ bacteria per milliliter. Initial adhesion experiments of the microorganisms were carried out in static mode at 37 °C. To avoid microbial sedimentation effect this was done with mild orbital agitation of 20 rpm for periods of 30, 60 and 90 minutes.

2.5.3 *Biofilm* formation on the surface of the coatings

For the biofilm formation assays, the bacteria were inoculated in BHI and grown overnight at 37 ºC. The bacterial concentration was adjusted by spectrophotometry until 62 % of transmittance (Helios epsilon model, Thermo Spectronic, Thermo Fisher Scientific Inc., Cambridge, UK) at 492 nm wavelength (λ), in order to obtain approximately $3x10^8$ CFU/mL. The samples were placed in 12-well plates and sterilized under ultraviolet light in a horizontal laminar air flow cabinet for 45 min. Then, to facilitate adhesion, 2 mL of bacterial suspension were placed in contact with the samples for 90 minutes at 37 ˚C. Subsequently non-adherent bacteria were carefully removed, and fresh sterile BHI was added and cultured for 24 hours at 37 ˚C in CO_2 atmosphere. After incubation, the samples were washed with BHI and viable bacteria in biofilm were quantified with the BacTiter-Glo™ Microbial Cell Viability Assay (Promega Corporation, Madison, WI, USA). 1mL of the BacTiter-Glo™ Reagent per sample was added and incubated in darkness for 10 min with gentle shaking (20 rpm). The supernatant was transferred to polystyrene opaque/white sterile microplates (Greiner Bio-one. Germany) and the light emission reaction (luciferin-luciferase) was measured by a luminometer (Microplate Fluorescent Reader FLX 800, Bio-Tek Instruments, USA). Each assay was repeated three times with different cultures in order to confirm reproducibility.

2.6 Image analysis

Images of cultured cells were acquired at 10x and 40x magnification (n = 10) (DAPI channel-nuclei, and FITC channel for OPN and IBSP detection). The images were analyzed and treated with Fiji-Image J software, transformed to an 8-bit grayscale bitmap and segmented using the Trainable Weka Segmentation plugin to create a binary mask. Total nuclei per image, focal adhesion or total expression of OPN and IBSP were quantified using the particle analysis command. Cell morphology was analyzed by calculation of different parameters using ImageJ software. Cell spreading area and roundness ($4 \times \text{area } \pi\text{-}1 \times [\text{major axis}]^2$) were calculated by evaluation of at least 20 cells for each condition. The quantification of bacteria adhering to different surfaces was carried out with six images per sample at 100x. The images were analyzed using NIS Elements Br software (Nikon Instruments Inc., NY, USA).

2.7 Statistical Analysis

All results are shown as mean ± standard deviation (SD). Contact angle, adhesion and differentiated cell quantification were analyzed using one-way ANOVA, with a Tukey's (multiple comparisons test) by Prims software. ANOVA test by IBM SPSS Statistics 19 software was used for bacterial initial adhesion evaluation. $p < 0.05$ was considered significant and indicated with an asterisk on each figure. SPSS Statistics 19 software and t-student test for independent samples was used for quantification of biofilm formation. All experiments were performed at least per triplicate.

3. Results and discussion

3.1 Substrate and coatings characterization.

Some properties of substrates and coatings such as microhardness, roughness and thickness are described in Table 3. AISI 316L stainless steel surface microhardness ostensibly rose from 2.50 GPa to 6.35 Gpa after plasma nitriding, due to solid solution hardening generated by the interstitial occupation of nitrogen in the cubic lattice of Fe-matrix and to the formation of hard Fe- and Cr- nitride, among other. Although the ceramic matrix TaN presented a hardness of 25 GPa, a mixed hardness of the multilayer coating ranged between 7.6 and 8.2 GPa, which is very appropriate as it leads to a smooth change of hardness from the substrate to the top layer, contributing to improved adhesion of the compound to the substrate. Microhardness decreased when the TaN coating was doped with Ag, possibly due to low hardness of silver and matrix deformation after Ag incorporation, which enabled breakage of the columns and the rearrangement of the compound, and thus a decrease in microhardness (54–56). In spite of the decrease in hardness with respect to the TaN matrix, all coatings with Ag inclusions had higher microhardness than AISI 316L stainless Steel.

The surface roughness of the steel sample increased after nitriding and be coated with TaN. This is due to the accommodation process of nitrogen and tantalum atoms in the steel surface, typical of magnetron sputtering technique. The roughness value increased with the bias voltage on the coating (57). This leads to more bombardments of ions with excessive modification to high mobilization in the substrate surface during the rise of this property (58).

Table 3. Properties of substrate and coatings, chemical composition, microhardness and thickness.

				Chemical Composition at%		
				After thermal treatment		
Sample $TaN_x(Ag)_y$	*Microhardness (GPa±SD)*	*Roughness (nm±SD)*	*Multilayer coating thickness (µm±SD)*	*Ta*	*N*	*Ag*
AISI 316L	*2.50±0.32*	*27±6*	-	-	-	-
Nitrided AISI 316L	*6.35±0.12*	*29±3*				
TaN (49)	*25.9±0.12*	*38±6*	*2.50±0.20*	*53.7*	*46.3*	-
30V-DL	*7.62±0.80*	*47±5*	*1.31±0.20*	*36.2*	*45.6*	*18.3*
60V-DL	*7.85±0.62*	*73±4*	*1.39±0.20*	*33.0*	*49.6*	*17.4*
90V-DL	*8.05±1.10*	*93±5*	*1.38±0.20*	*33.7*	*49.8*	*16.5*
120V-DL	*8.19±0.72*	*125±7*	*1.38±0.20*	*33.9*	*49.8*	*16.5*

The higher the bias voltage the greater the density of the coating, due to the intense ion bombardment of the surface. The amount of silver decreased when the bias voltage rose, because in dense films there are fewer spaces that permit silver diffusion after thermal treatment. On the other hand, the silver content decreased due to the re-sputtering phenomenon of silver (59).

Figure 2a shows the TaN coating surface with quasi-spherical grains with globular domes (60). Ag nano-clusters can be observed in the surface of the TaNx(Ag)y coating without diffusion layer and after the heat treatment as shown in Figure 2b. Samples provided with a TaN diffusion top layer and heat treated (Figure 2c shows 30V-DL surface) exhibited a decreased number of Ag nano-clusters, as explained above, and a change in the surface topography is apparent.

XRD patterns for TaNx(Ag)y multilayer coatings are shown in Figure 2d. This spectrogram presents the peaks of the crystalline phases of face centered cubic (fcc) TaN grown in (111), (200) and (220) directions, as well as independent peaks of silver with preferential growth in directions (111) and (200). However, their intensity is very low, due probably to the low silver content on the top diffusion layer and to the nano size of silver particle. This result indicates the insolubility of this element in the TaN matrix without intermetallic compounds formation. This behavior is presented in the structural zone model (SMZ) by *Bhatnagar* and *Adamik* (61,62).

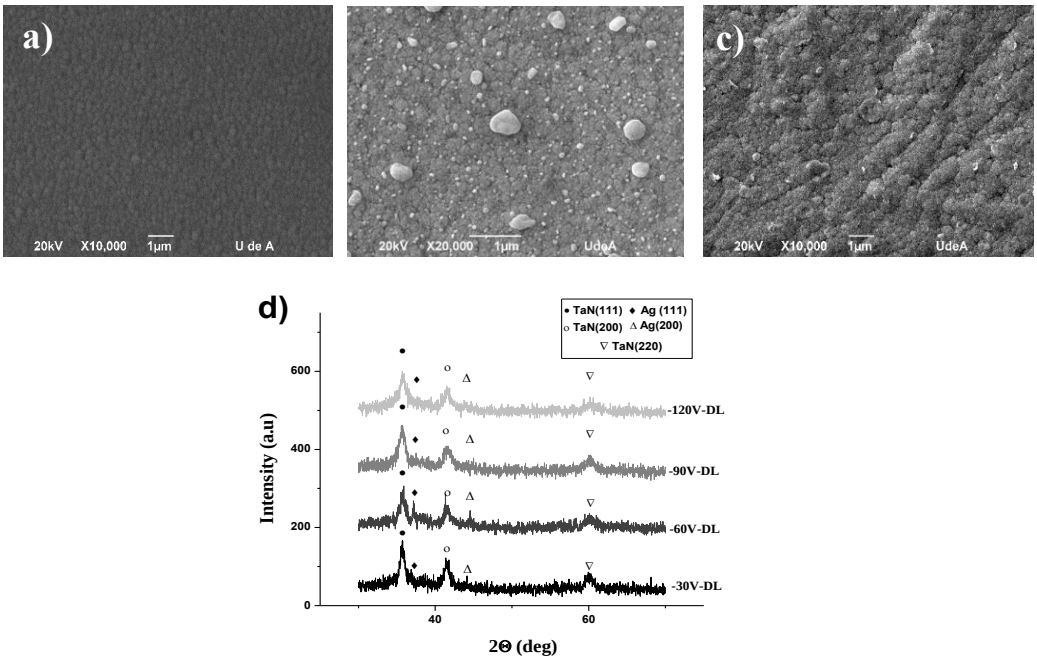

Figure 2. SEM superficial micrographs (a) TaN coating, (b) TaNx(Ag)y coating without TaN diffusion layer after heat treatment and (c) 30V-DL coating with TaN diffusion layer after heat treatment. (d) XRD patterns for TaNx(Ag)y multilayer coatings with different bias voltage applied to diffusion top layer.

The average size of the silver nanoparticles (Ag-NPs) of the deposited coatings was determined by Atomic Force Microscopy (AFM) equipped with a device MFP-3D-Oxford Instruments Asylum Research in resistive mode, as shown in Figure 3. In Figure 3a, it was observed that the Ag-NPs size larger than 100nm, increased with increasing bias voltage applied to the substrate and after heat treatment of the coated samples, which presented minimum values of 62.77 ± 17.31nm and maximum of 182.48 ±88.52nm for the sample 30V- DL. The frequency of Ag-NPs with sizes between 20 and 100 nm are very similar for all coatings. Likewise, the grain size of the TaN- matrix was measured,

which decreased with increasing bias voltage. 120V- DL coating presents the mayor value in number of nanoparticles with size greater than 100nm in contrast with 30V-DL coating, showed on the tope line micrographs in Figure 3b.

TaN diffusion layer grain size, decreased when the bias voltage rises as shown on the bottom line of micrographs in Figure 3b. This result suggests that the greater proximity between the grain boundaries of the structure with smaller grain size (for sample 120V-DL) obstructs the process of diffusion of silver and thus decreases the rate of ion release to the environment SBF (as discussed below), but it favors the coalescence of the Ag nanoparticles found on the surface, increasing their size and decreasing their frequency; the silver coalescence phenomenon in TaN(Ag) coatings after thermal treatment was evidenced in previous work, and the same way the properties before annealing (48).

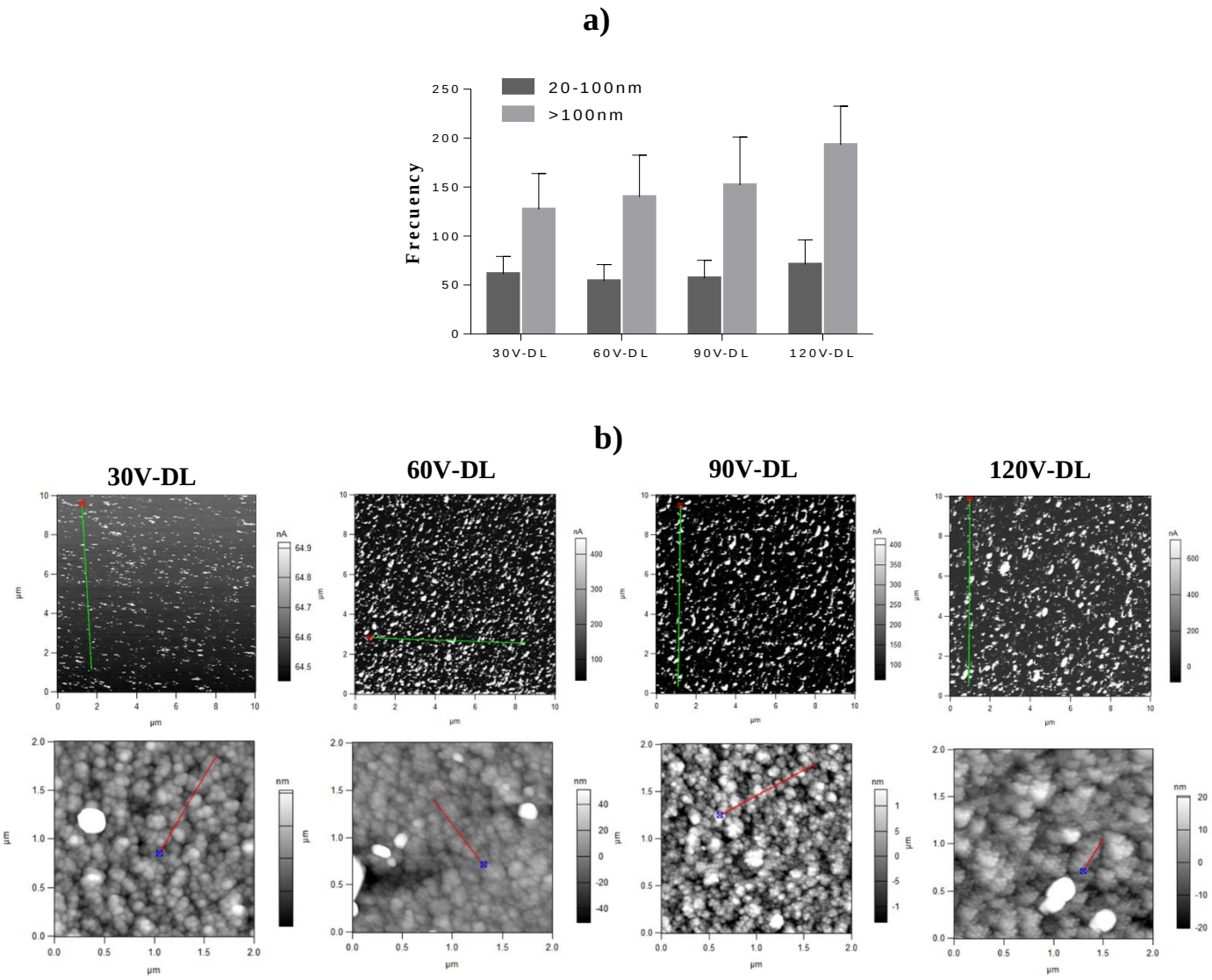

Figure 3. a) Ag-NPs size, (data expressed as a mean ± standard deviation), b) Ag-NPs detection by conductive mode AFM - Pt tip (on the top line), and grain size (on the bottom line), as a function of the bias voltage applied during the deposition of the TaN diffusion layer.

The Ta adhesion layer between the substrate and the 30V-DL coating can be seen in the FIB micrograph (Figure 4a). This monolayer has a thickness of 64.86 ± 3.41nm. In EDX analysis of the 30V-DL coating cross section

indicated in Figure 4b, it is shown that Ag diffuses towards the surface, staying between TaN matrix grains boundaries and in the direction of free gaps in the Ta adhesion layer.

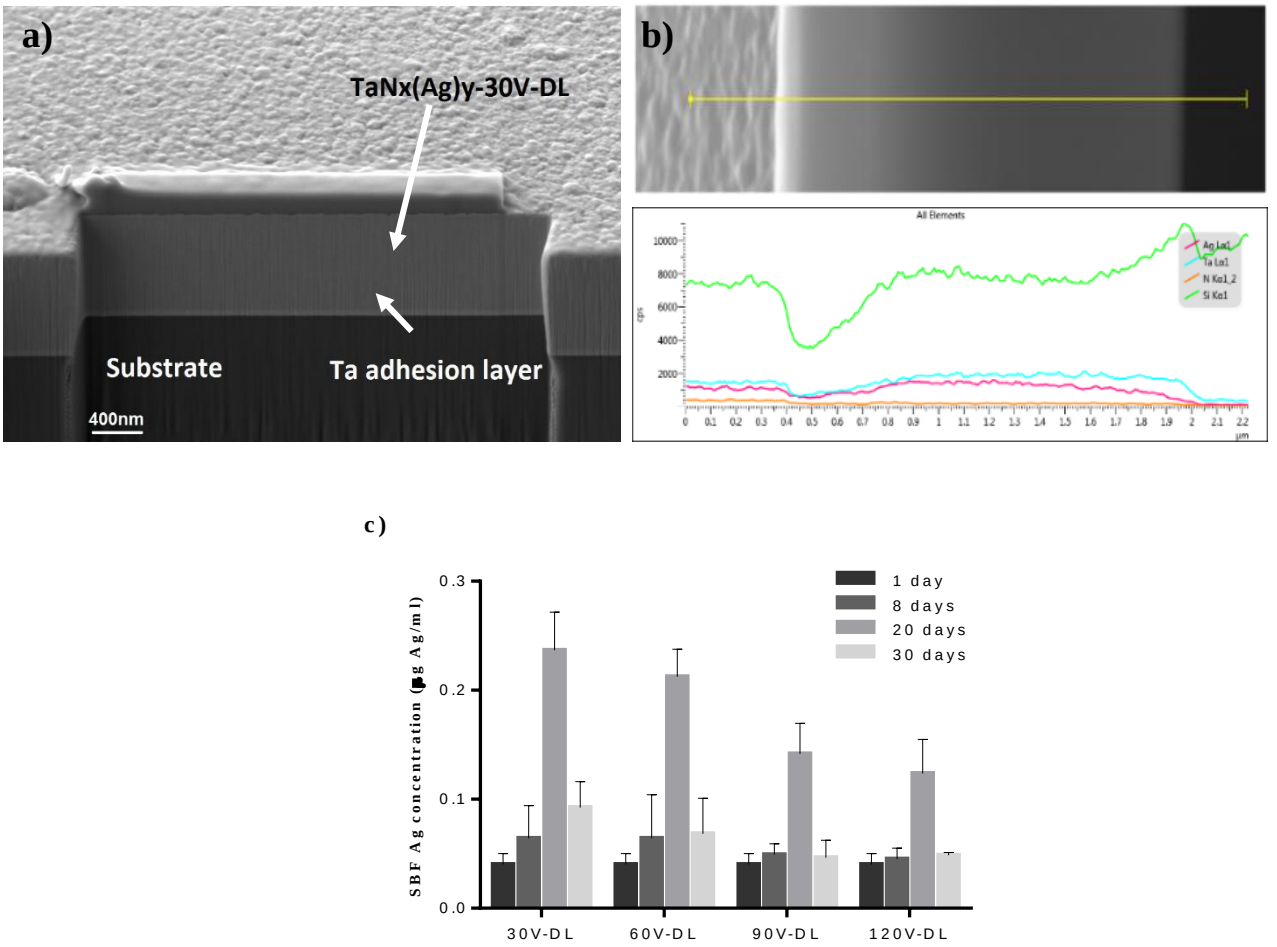

Figure 4. (a) FIB-FESEM cross sectional image and (b) EDX analysis of the 30V-DL coating. (c) Ag release assay in SBF medium detected by MIP for the different TaNx(Ag)y multilayer coatings, at times of 20 and 30 days expressed as a mean ± standard deviation.

Ag concentration values in SBF after release assays for the different TaNx(Ag)y multilayer are shown in Figure 4c. It can be clearly seen that Ag content decreases in the SBF solution as the applied bias voltage in the samples increases. It is interesting to note that the amount of Ag released into the medium was higher after 20 days than after 30 days. These results seem to be correlated with the fact that the diffusion layer is more dense when the bias voltage increases, allowing the high attraction and accommodation of ions on the substrate surface during coating formation, according to some authors and previous works to this (58,59,48). The release of Ag into the surrounding medium is directly related to the size and density of nanoparticles on the substrate surface indicating that smaller nanoparticles have a larger surface area of contact with the medium that makes them highly reactive as the case of the coating

deposited at a bias of -30V (-30V-DL sample) that showed increased release of this metal; otherwise it occurs with -120V-DL coating whose nanoparticles showed greater size and lower reactivity disfavoring the release of Ag.

Surface energy and contact angle of the substrate with the different coatings are summarized in Table 4 and showed in Figure 5. According to *Żenkiewicz* and other authors, when the surface energy has a positive value and the contact angle is lower than 90°, the surface has an hydrophilic character (50,52,53).

Table 4. Θ_W, Θ_G, Θ_F contact angles to water, formamide and glycerol, and surface energy components: polar (γsp), dispersive (γsd) and total surface energy (γs) of the AISI 316L and coatings.

Sample	*Contact angle* ±SD (deg)			*Surface energy components (mJm^{-2})*		
	Θ_W	Θ_G	Θ_F	γ_s^p	γ_s^d	γ_s
AISI 316L	*92.6±3.6*	*86.5±5.2*	*81.6±1.8*	5.6	15.4	21.0
30V-DL	*64.8±7.6*	*66.3±5.9*	*68.4±7.0*	0.0	73.2	73.2
60V-DL	*59.6±4.2*	*62.2±6.7*	*45.3±2.3*	52.7	0.4	53.1
90V-DL	*55.7±2.2*	*75.4±6.2*	*62.3±1.4*	0.0	73.2	35.2
120V-DL	*51.9±1.4*	*72.1±4.3*	*64.7±3.6*	6.4	28.8	30.1

The surfaces of the coatings have hydrophilic behavior, but the AISI 316L stainless steel presented a water contact angle of 92.6 ± 3.6 in the hydrophilic-hydrophobic limit (Figure 5a). However, its surface energy is lower and positive, thus its surface has a tendency to be wet (Figure 5b). These results can be explained by the fact that TaNx(Ag)y multilayer coating roughness increased with the bias voltage rise in the diffusion layer development (Table 3). This suggests a less homogeneous granular structure formation, hence a smaller active surface area and as a result smaller surface energy. These results are in line with previous works (58,63).

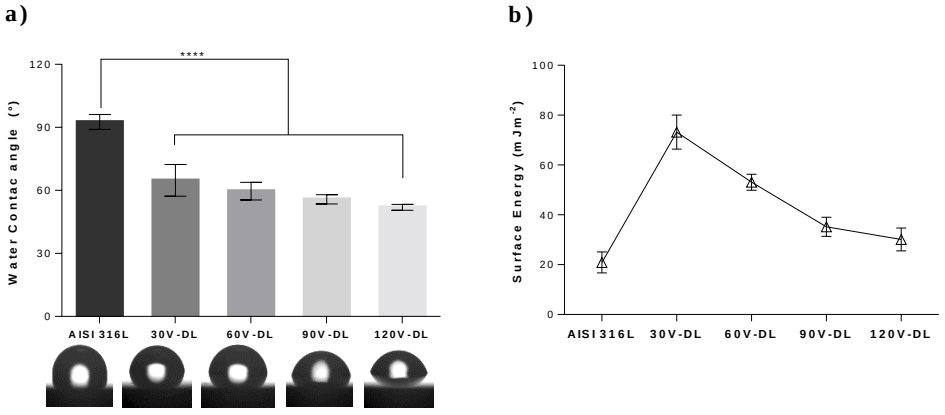

Figure 5. (a) Water contact angle and (b) total surface energy of AISI 316L of the different TaNx(Ag)y multilayer coatings expressed as a mean ± standard deviation. Significant values as ****p < 0.0001.

3.2 Biocompatibility response on TaNx(Ag)y multilayer coatings

3.2.1 Cell adhesion

Cells were cultured for 3 h to evaluate the initial adhesion of pre-osteoblast grown onto different coatings and the AISI 316L stainless steel control surface (Figure 6). The development of actin cytoskeleton and vinculin detection

as a marker of focal adhesion protein was investigated as a function of the different coatings utilized. The state of F-actin cytoskeleton was well developed in cells cultured on the AISI 316L control, 30V-DL and 60V-DL coatings, showing spread morphology of cells and stress fibers of actin. In contrast, the 90V-DL and 120V-DL coatings presented minimal levels of cytoskeleton formation although staining corresponding to initial stages of F-actin polymerization is clearly visible (Figure 6a) on cells presenting a rounded morphology (Figures 6a and b). Focal adhesion formation, necessary for cell adhesion, occurs and subsequent integrin clustering takes place after the formation of stable links between the extracellular matrix proteins and the actin cytoskeleton (64).

Well defined focal adhesions were formed on the control AISI 316L and 30V-DL, 60V-DL coatings, consequent to the development of actin cytoskeleton. In contrast, vinculin is not organized into focal adhesions on the 90V-DL and 120V-DL coatings, but randomly distributed throughout the cell (Figure 6a). The results showed that cell morphology strongly depends on the different configurations of diffusion layers obtained for different coatings. Dense configuration of diffusion layer was obtained for 90V-DL and 120V-DL coatings on which silver released to the medium is lower compared to 30V-DL and 60V-DL coatings (Figure 2) suggesting that the amount of Ag for 90V-DL and 120V-DL coatings remains anchored to the surface increasing the roughness of coatings as well as being in direct contact with cells. Thus, cell morphology strongly depends on the presence and amount of Ag particles on the coatings and cells tend to be rounded and lacking defined focal contacts.

Cell spreading area and circularity parameters were calculated by image analysis, and the results are shown in Figure 6c and d. The results indicated a remarkably linear relationship among different bias voltages applied to the diffusion layer for different coatings compared to the steel substrate control; spreading area decreases and cell circularity increases respectively on substrates 90V-DL and 120V-DL (Figures 6c and d). These results are consistent with those obtained regarding cytoskeleton formation and vinculin detection (Figure 6a) and in line with other works previously reported (65).

Quantification of focal adhesions showed higher protein levels on cells grown onto AISI 316L stainless steel control and 30V-DL substrates compared with 60V-DL, 90V-DL and 120V-DL substrates that presented minimum levels (Figure 6e). Indeed, AISI 316L and 30V-DL substrates presented higher focal adhesion frequency (Figure 6f) of mature focal adhesions (> 6 μm^2) and the frequency increased even more in terms of nascent focal adhesions (< 2 μm^2) for 30V-DL substrate, suggesting optimal adhesion efficiency.

The results are in line with those obtained in previous works indicating that topography strongly affects the cell adhesion process (66,67). On 60V-DL, 90V-DL and 120V-DL coatings, greater Ag nanoparticles are on the surface of the coating, thus conferring both an increased roughness (Table 3) and more Ag in contact with cells a fact that seems to reduce initial cell adhesion in terms of cytoskeleton and focal adhesion contacts development as well as producing severe morphological changes as previously reported (65,68–71).

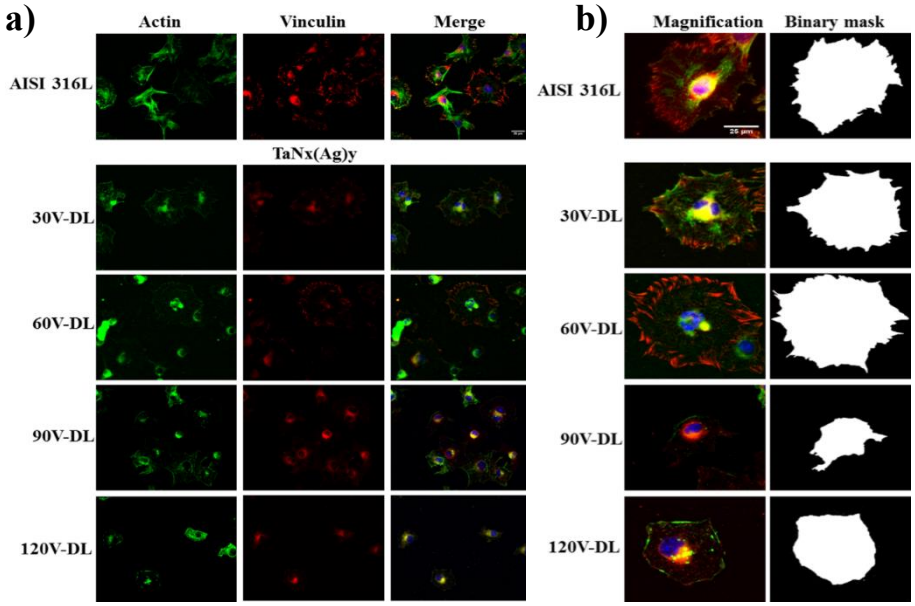

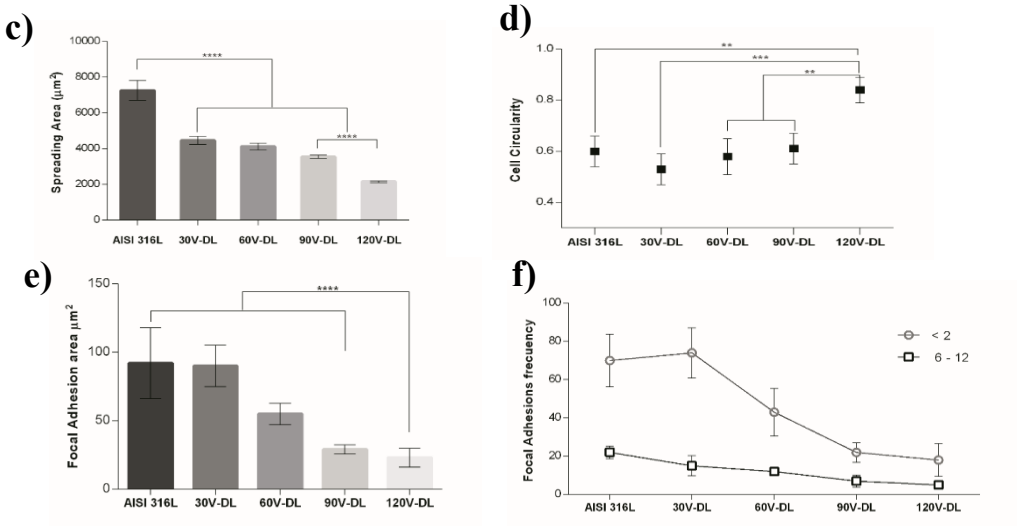

Figure 6. (a) Adhesion of MC3T3-E1 cells on the different coatings and AISI 316L stainless steel control after 3 hours of culture. The first column shows F-actin cytoskeleton (green) and the second one vinculin (red). Nuclei were counter stained with DAPI (scale bar 25 µm). (b) Representation of the sequential process and binary mask creation followed for calculations of spreading area and circularity parameters (scale bar is 25 µm). (c) Analysis of spreading area and (d) cell circularity. (e) Quantification of focal adhesion area on cells cultured on different substrates. (f) Frequency of focal adhesion size. Data is represented as mean ± standard deviation. Significant values as ****p < 0.0001, ***p < 0.001, **p < 0.01.

3.2.2 Cell differentiation

In order to investigate possible long-term effects of the Ag content of the different coatings and the potential ability of the cells to stimulate subsequent growth of bone tissue, we evaluated cell differentiation by means of detection of expression of different genes as markers of osteogenesis. These were Osteopontin (OPN) and Integrin Binding Sialoprotein (IBSP). OPN is an osteoblast specific gene that promotes osteoblast phenotype and its expression produces a secreted adhesive protein that plays a key role in cell adhesion, migration and survival (72). IBSP is a glycosylated protein present within bone matrix. The protein is characterized by its ability to bind to hydroxyapatite, indicating its potential role in the early mineralization of osteoblasts. In addition, IBSP can promote pre-osteoblast differentiation into mature osteoblasts, stimulating bone mineralization (72).

MC3T3-E1 cells were induced to differentiate using osteogenic differentiation medium. After 15 days of culture, protein detection was performed by immunofluorescence with specific antibodies against OPN and IBSP. Intensity of staining is shown in Figure 7. Both control steel and 30V-DL substrates presented higher levels of OPN and IBSP staining when compared with the 60V-DL, 90V-DL and 120V-DL coatings (Figures 7a and c). Again, this

indicates a strong dependence of cell function on the presence of surface Ag nanoparticles, increasing detection of differentiation markers as the roughness of the coatings diminishes. Furthermore, long term viability of the samples seems to be affected, resulting in a decrease in the total number of cells present in the samples and compared to control steel (Figure 7b).

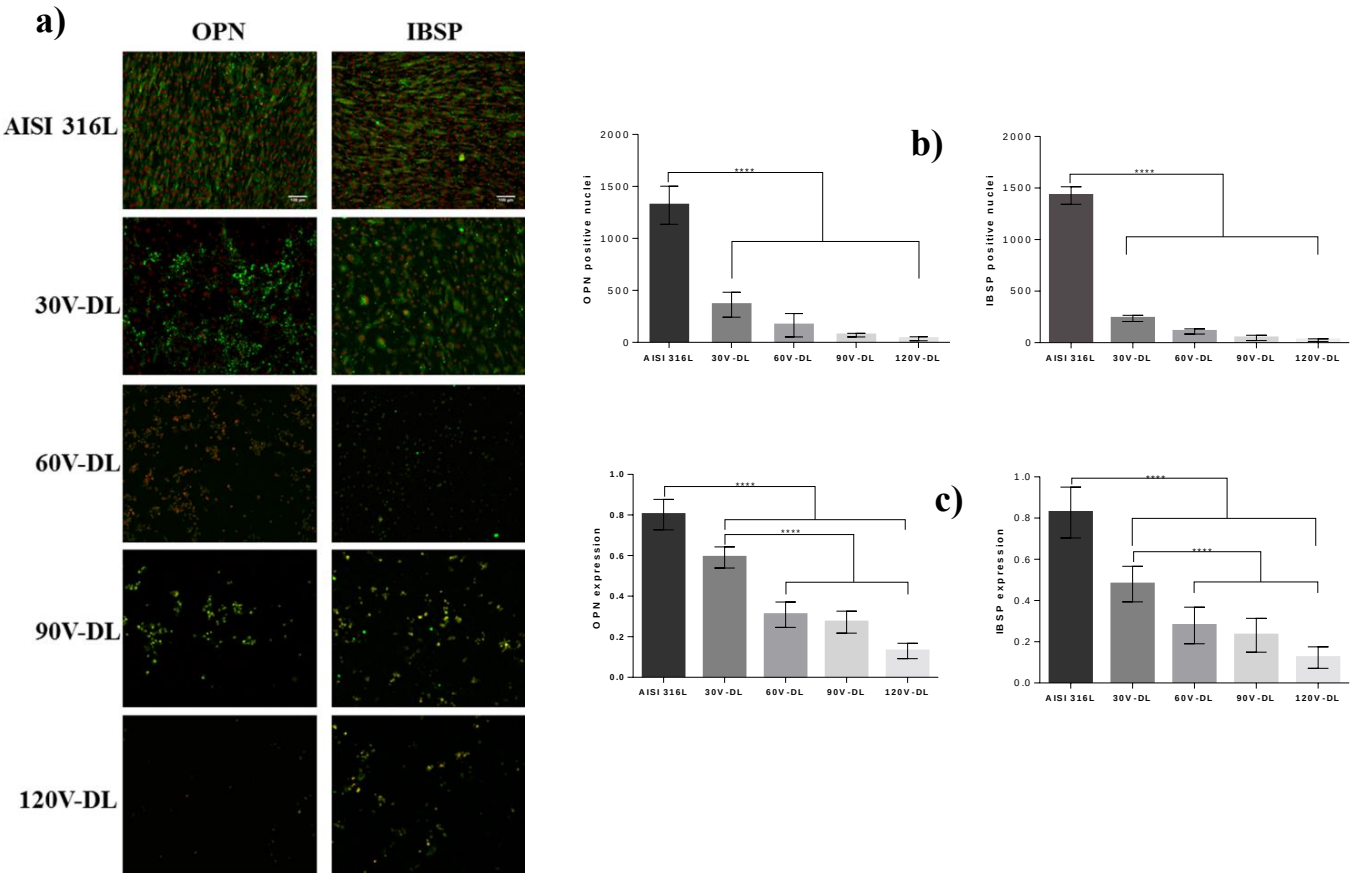

Figure 7. (a) Fluorescence microscopy images showing expression of Osteopontin (OPN, green), Integrin Binding Sialoprotein (IBSP, green) and nucleus (red). Scale bar 100 μm. (b) Quantification of number of cells grown onto different substrates. (c) Image analysis quantification of OPN and IBSP staining. Data was represented as mean ± standard deviation. Significant values are represented as ****$p < 0.0001$.

Quantification of staining levels after long term culture for both differentiation markers (OPN and IBSP) was high enough even though the final number of cells present on the 30V-DL coating was lower than the steel control surface. This suggests that 30V-DL coating is capable of inducing proper cell differentiation behavior in the long term. These results are in line with those obtained in cell adhesion experiments (Figure 6). The fact that 60V-DL, 90V-DL and 120V-DL coatings presented a minimal cell number after 15 days of culture could be explained if it is considered that cell growth on these samples shows a delay in initial cell adhesion and spreading, and consequently this phenomenon is affecting cell differentiation as well. Furthermore, the topography generated by the presence of Ag nanoparticles on the surface of the coatings results in a significant decrease in osteoblast differentiation markers, as has been previously reported (73).

Overall, our results indicate that the 30V-DL coating could maintain optimum levels of osteoblast cell adhesion at the beginning of the surgical intervention, achieving cell differentiation in the long term. This would benefit osseointegration processes during the recovery times of implant patients.

3.3 Bacteria-response on AISI 316L stainless steel and TaNx(Ag)y multilayer coatings

3.3.1 Quantification of adhered bacteria

In all surfaces, a growing trend was observed in the adhesion of microorganisms as the adhesion time increased, as shown in Figure 8. No significant differences were found between the different coatings and the AISI 316L stainless steel, with the exception a little diminution in of the 30V-DL surface. At contact times longer than 30 minutes there is a statistically significant diminution in the bacteria number only on the 30V-DL coating, probably produced because this coating is the surface that delivers the greatest amount of Ag into the surrounding medium. This seems to reduce the microorganism adhesion produced in the solid-liquid interface between coating and suspension, decreasing the number of adherent bacteria on its surface. Nevertheless, in several works including that discussed by *Abraham Rodríguez-Cano et*. al, it is described that bactericidal effect did not appear until 200 minutes of assay for staphylococcus strain (71) indicating that the 30V-DL surface could show an advantage in the potential bactericidal effect in times over 90 minutes (74–76).

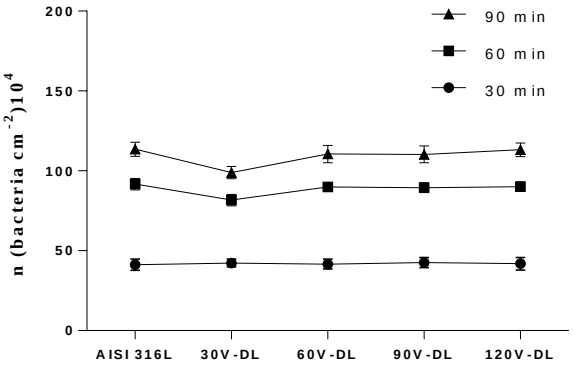

Figure 8. Total number of adhered *Streptococcus sanguinis* ATCC10556 bacteria on AISI 316L stainless steel surface and TaNx(Ag)y multilayer coatings as a function of contact time.

According to the results reported by *Wan et. al*, microorganism adhesion is a high complex process, related to properties that influence physicochemical interactions like wettability, roughness and surface chemistry (77). Some reports showed that *Streptococcus sanguinis* tend to adhere more easily to surfaces with low surface energies, which agrees with the results obtained for water contact angle in this study (78–81). However, whether adhesion of bacteria to the surface is favored or not depends not only on the physicochemical properties of the surface material but also on the nature of the bacterial strain (82).

3.3.2 Evaluation of biofilm formation on AISI 316L stainless steel and TaNx(Ag)y multilayer coatings

After 24 hours of culture, a considerable reduction of the viability of the biofilm in the 30V-DL coating was observed in comparison with the AISI 316L stainless steel and the other coatings, as showed in Figure 9. Surface roughness seems to be a determining factor in the adhesion of bacteria (83), which explains the linear relationship with bias voltage in the diffusion layer applied to coatings. This could be directly related to the fact that biofilm formation is favored on rough surfaces, as a consequence of the increase in the surface area, the presence of more sites (depressions) for colonization and an ideal medium to protect the biofilm from the mechanisms of environmental self-cleaning (84,85).

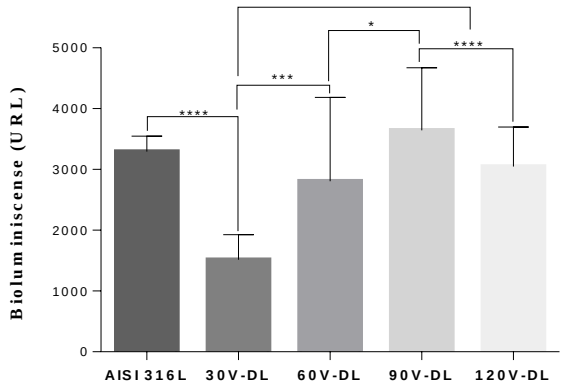

Figure 9. Bacterial biofilm viability of *Streptococcus sanguinis* ATCC 10556 after 24 hours of culture on AISI 316L stainless steel surface and TaNx(Ag)y multilayer coatings. Significant values are represented as ****$p < 0.0001$

Based on the results, we hypothesized that during the high release of Ag from 30V-DL coating to the surrounding medium due to high reactivity (high surface area) of Ag nanoparticles with smaller sizes, strongly affected reduction of biofilm formation, as previously described due to the strong oxidative activity of the Ag ions, when they are in direct contact with the bacterial wall (32,86). Recently, many investigations have tried to elucidate the mechanisms by which silver nanoparticles inactivate processes necessary for bacteria viability. Some authors argue that Ag nanoparticles directly denature bacterial DNA thus compromising bacterial ability to replicate (87). Others argue that once the nanoparticles come into contact with the bacteria wall, they induce the formation of irreversible complexes such as sulfhydryl orhistidyl, inactivating the life processes of bacteria such as deshydro-oxygenation (88,89).

In our case, the measurement of released Ag from the coatings indicated that in all cases the Ag concentrations were lower than 0.25 µg/mL. Although Ag cytotoxicity levels are still the subject of study, previous investigations report values of 30 µg/mL as a minimum cytotoxic concentration in human fibroblast at 24 hours (90) or 31.75 µg/mL (91) and concentrations higher than 44µg/mL induce cell apoptosis (92). Ag release measurements results showed a strong dependence on bias voltage; as this increases, the amount of silver in the medium decreases explained by the degree of compaction and densification acquired by the film as this variable increases.

The greatest concentration value of Ag released is detected at 20 days in all the coatings tested and the maximum value of release is presented in the 30V-DL coating with 0.23 µg/mL, value even lower than those reported as cytotoxic. Ag liberation from 30V-DL coating during the first 8 days is minimal, representing an advantage for dental applications because in the period of healing of increased susceptibility, the patient will not be affected by the Ag release from metal. Indeed, concentrations of Ag released from 30V-DL coating are high enough to minimize biofilm formation, without being cytotoxic according to results obtained for MC3T3-E1 cells.

Finally, proposed design for development of TaNx(Ag)y multilayer coatings resulted in increased biocompatible properties and a decreased bacterial adhesion caused by bacterial damage generated by Ag presence, conferring to this system capability for dental implant applications. The Ag nanoparticles embedded in the matrix, and their release into the biological medium, could ensure a long-term antibacterial or bacteriostatic effect due to the conformation of the diffusion layer (93) that constitutes a reserve for this purpose without affecting cell regeneration during the recovery times of patients. In general terms for the different properties evaluated in the present work, a strong influence due to the increase in bias voltage during the manufacture of the diffusion layer causing an increment in roughness, decreased of release of Ag to the surrounding medium and a change in the wettability of steel. The combinations of the different effects produced by bias voltage upon the biological response of materials affected positively cell viability negatively affected biofilm formation. 30V-DL coating could be the most promising candidate for biomedical applications, showing the best balance between biocompatibility and antibacterial effect.

4. Conclusions

The main aim of this work was to improve the bio-response of AISI 316l stainless steel through the deposition of TaNx(Ag)y nanocomposite duplex coatings, developed through the combination of pulsed plasma nitriding and unbalanced magnetron sputtering techniques. A fundamental role in the multi-layer coating system played the diffusion top layer, whose thickness, surface topography and density can be controlled by the bias voltage supplied to it, and markedly influences on the biological properties of the entire coating system.

MC3T3 osteoblastic cells were cultured on the coated substrates to evaluate biocompatibility, and the *Streptococcus sanguinis* ATCC 10,556 strain was used to assess antimicrobial effect. The results obtained after microstructural and biological evaluation of the coated steel samples showed a correlation between the variations in bias voltage applied to the diffusion top layer the different coatings with Ag release kinetics, as well as roughness and surface wettability. The smaller grain size of the TaN diffusion layer with increasing bias voltage established that the closeness of the grain boundaries in this structure promotes coalescence of Ag nanoparticles which diffused and emerged to the sample surface after heat treatment increasing their, and thus generating a greater area of contact with osteoblast cells decreasing their bio-response. The small size and higher density per unit area of Ag nanoparticles in the coating 30V-DL allowed a significant reduction of biofilm formation and bacterial adhesion.

In terms of osteogenic induction, lower bias voltages applied during the deposition of the diffusion layer of the TaNx(Ag)y coatings allowed a greater release of Ag to the medium and lower surface roughness and wettability. This improved the process of adhesion and differentiation of the osteoblastic cells on the surface of the top diffusion layer deposited with 30V-DL. On the other hand, the *Streptococcus sanguinis* ATCC 10,556 strain showed low adhesion and biofilm formation in comparison with the uncoated steel for the same surface and under the same test conditions. The 30V-DL coating showed the most promising behavior, as it exhibited an appropriated balance between biocompatibility and bacterial adhesion, making it the most suitable material for use in biomedical applications.

Acknowledgments

The authors are grateful to ‘‘Departamento Administrativo de Ciencia, Tecnología e Innovación COLCIENCIAS’’, University of Antioquia for financial assistance with the Project contract No. 0940-2012, to Becas Santader and Enlazamundos program. Also thank to FIB-FESEM and EDX analysis was performed under the technical guidance of the Microscopy Service of the Universitat Politècnica de València, whose advice is greatly appreciated.

The financial support from the Spanish Ministry of Economy and Competitiveness (MINECO) (through the MAT2015-69315-C3-1-R) and FEDER funds project are acknowledged. CIBER-BBN is an initiative funded by the VI National R&D&I Plan 2008-2011, Iniciativa Ingenio 2010, Consolider Program, CIBER Actions and financed by the Instituto de Salud Carlos III with assistance from the European Regional Development Fund.

References

1. Cooper LF, Masuda T, Whitson SW, Yliheikkilä P, Felton D a. Formation of mineralizing osteoblast cultures on machined, titanium oxide grit-blasted, and plasma-sprayed titanium surfaces. Int J Oral Maxillofac Implants. 1999;14(1):37–47.
2. Chu PK. Surface engineering and modification of biomaterials. Thin Solid Films. 2013 Jan;528:93–105.
3. Rodríguez Rius D, García Saban FJ. Physico-chemical characterization of the surface of 9 dental implants with 3 different surface treatments. Med Oral Patol Oral Cir Bucal. 2005;10(1):58–65.
4. Menthe E, Bulak A, Olfe J, Zimmermann A, Rie K. Improvement of the mechanical properties of austenitic stainless steel after plasma nitriding. Surf Coat Technol. 2000;259–63.

5. Fewell MP, Mitchell DRG. The nature of expanded austenite. Surf Coatings Technol. 2000;131(1–3):300–6.

6. Ratner B, Hoffman A, Schoen F, Lemons J. Biomaterials Science: an introduction to materials in medicine. Estados Unidos: Academic Press; 1996. 11-22 p.

7. Balla VK, Banerjee S, Bose S, Bandyopadhyay A. Direct laser processing of a tantalum coating on titanium for bone replacement structures. Acta Biomater. 2010;6(6):2329–34.

8. Matsuno H, Yokoyama A, Watari F, Uo M, Kawasaki T. Biocompatibility and osteogenesis of refractory metal implants, titanium, hafnium, niobium, tantalum and rhenium. Biomaterials. 2001;22(11):1253–62.

9. Zardiackas LD, Kraay MJ, Freese HL. Titanium, Niobium, Zirconium, and Tantalum for Medical and Surgical Applications. Library. 2012.

10. Bernoulli D, Müller U, Schwarzenberger M, Hauert R, Spolenak R. Magnetron sputter deposited tantalum and tantalum nitride thin films: An analysis of phase, hardness and composition. Thin Solid Films. 2013 Dec;548:157–61.

11. Bouchet-Fabre B, Pinault M, Foy E, Hugon MC, Minéa T, Mayne-L'Hermite M. Interface study between nanostructured tantalum nitride films and carbon nanotubes grown by chemical vapour deposition. Appl Surf Sci. 2014;315:510–5.

12. Zhou Y, Jin P, Chen S, Zhu Y. Tantalum nitride nanowires: Synthesis and characterization. Mater Lett. 2014;136:168–70.

13. Hwan J, Yeon H, Chan S, Hye D, Keun B, Park J, et al. Growth of tantalum nitride film as a Cu diffusion barrier by plasma-enhanced atomic layer deposition from tantalum complex. Appl Surf Sci. 2016;362:176–81.

14. Bromark M, Larsson M, Hedenqvist P, Hogmark S. Mechanical and tribological characterization of DC magnetron sputtered tantalum nitride thin films. Surf Coatings Technol. 1997;97:779–84.

15. Saha R, Barnard J a. Effect of structure on the mechanical properties of Ta and Ta(N) thin films prepared by reactive DC magnetron sputtering. J Cryst Growth. 1997;174:495–500.

16. Riekkinen T, Molarius J, Laurila T, Nurmela A, Suni I, Kivilahti JK. Reactive sputter deposition and properties of TaxN thin films. Microelectron Eng. 2002;64:289–97.

17. Stavrev M, Fischer D, Wenzel C, Drescher K, Mattern N. Crystallographic and morphological characterization of reactively sputtered Ta, TaN and TaNO thin films. Thin Solid Films. 1997;307:79–88.

18. Akao SN, Umata MN, Hmi TO. Thin and Low-Resistivity Tantalum Nitride Diffusion Barrier and Giant-Grain Copper Interconnects for Advanced ULSI Metallization. Jpn JAppl Phys. 2401:4–9.

19. Radhakrishnan K, Geok N, Gopalakrishnan R. Reactive sputter deposition and characterization of tantalum nitride thin films. 1999;57:224–7.

20. Nie HB, Xu SY, Wang SJ, You LP, Yang Z, Ong CK, et al. Structural and electrical properties of tantalum nitride thin films fabricated by using reactive radio-frequency magnetron sputtering. Appl Phys A Mater Sci Process. 2001 Aug;73(2):229–36.

21. Pino J. "Estudio nanométrico de biocompatibilidad y adhesividad celular a biomateriales utilizados en cirugía ortopédica." Santiago de Compostela; 2008.

22. Hsieh JH, Yeh TH, Li C, Chiu CH, Huang CT. Antibacterial properties of TaN–(Ag,Cu) nanocomposite thin films. Vacuum. 2013 Jan;87:160–3.

23. Masini BD, Stinner DJ, Waterman SM, Wenke JC. Bacterial adherence to suture materials. J Surg Educ. 2011;68(2):101–4.

24. Dowling D., Betts A., Pope C, McConnell M., Eloy R, Arnaud M. Anti-bacterial silver coatings exhibiting enhanced activity through the addition of platinum. Surf Coatings Technol. 2003 Jan;163–164:637–40.

25. Kim J, Cho M, Oh B, Choi S, Yoon J. Control of bacterial growth in water using synthesized inorganic disinfectant. Chemosphere. 2004 May;55(5):775–80.

26. Lok CN, Ho CM, Chen R, He QY, Yu WY, Sun H, et al. Proteomic analysis of the mode of antibacterial action of silver nanoparticles. J Proteome Res. 2006;5:916–24.

27. Yoshinari M, Oda Y, Kato T, Okuda K. Influence of surface modifications to titanium on antibacterial activity in vitro. Biomaterials. 2001;22:1–2.

28. Search H, Journals C, Contact A, Iopscience M, Address IP. Ag – Ti (C , N) -based coatings for biomedical

applications : influence of silver content on the structural properties. J Phys D Appl Phys. 2011;375501.

29. Ostad SN, Dehnad S, Nazari ZE, Fini ST, Mokhtari N, Shakibaie M, et al. Cytotoxic activities of silver nanoparticles and silver ions in parent and tamoxifen-resistant T47d human breast cancer cells and their combination effects with tamoxifen against resistant cells. Avicenna J Med Biotechnol. 2010;2(4):187–96.

30. Stone V, Nowack B, Baun A, van den Brink N, von der Kammer F, Dusinska M, et al. Nanomaterials for environmental studies: Classification, reference material issues, and strategies for physico-chemical characterisation. Sci Total Environ. 2010;408(7):1745–54.

31. Hsieh JH, Tseng CC, Chang YK, Chang SY, Wu W. Antibacterial behavior of TaN–Ag nanocomposite thin films with and without annealing. Surf Coatings Technol. 2008 Aug;202(22–23):5586–9.

32. He W, Zhou YT, Wamer WG, Boudreau MD, Yin JJ. Mechanisms of the pH dependent generation of hydroxyl radicals and oxygen induced by Ag nanoparticles. Biomaterials. 2012;33(30):7547–55.

33. Alonso A. Development of polymeric nanocomposites with enhanced distribution of catalytically active or bactericide nanoparticles. Universidad Autónoma de Barcelona; 2012.

34. Bowker M. A prospective: Surface science and catalysis at the nanoscale. Surf Sci. 2009;603(16):2359–62.

35. Cai S, Xia X, Xie C. Research on Cu2+ transformations of Cu and its oxides particles with different sizes in the simulated uterine solution. Corros Sci. 2005 Apr;47(4):1039–47.

36. Schwartz A, Devorah D, Laviv, Amir L, DMD L. Failure Causes, Timing, and Cluster Behavior: An 8-Year Study of Dental Implants. Implant Dent. 2008;17(2):200–2007.

37. Kourtis S, Sotiriadou S, Voliotis S, Challas A. Private practice results of dental implants. Part I: survival and evaluation of risk factors—Part II: surgical and prosthetic complications. Implant Dent. 2004;13:373–85.

38. Duske K, Jablonowski L, Koban I, Matthes R, Holtfreter B, Sckell A, et al. Cold atmospheric plasma in combination with mechanical treatment improves osteoblast growth on biofilm covered titanium discs. Biomaterials. 2015;52(1):327–34.

39. Jang J, Lim D-H, Choi I-H. The impact of nanomaterials in immune system. Immune Netw. 2010;10(3):85–91.

40. Mombelli A, Müller N, Cionca N. The epidemiology of peri-implantitis. Clin Oral Implants Res. 2012;6:67–76.

41. Mager D, Ximenez-Fyvie L, Haffajee A, Socransky S. Distribution of selected bacterial species on intraoral surfaces. J Clin Periodontal. 2003;30(7):644–54.

42. Rosan B, Lamont R. Dental plaque formation. Microbes Infect. 2000;2(13):1599–607.

43. Xin Y, Liu C, Huo K, Tang G, Tian X, Chu PK. Corrosion behavior of ZrN/Zr coated biomedical AZ91 magnesium alloy. Surf Coatings Technol. 2009;203(17–18):2554–7.

44. Merl DK, Panjan P, Čekada M, Maček M. The corrosion behavior of Cr-(C,N) PVD hard coatings deposited on various substrates. Electrochim Acta. 2004;49(9–10):1527–33.

45. William Grips VK, Barshilia HC, Selvi VE, Kalavati, Rajam KS. Electrochemical behavior of single layer CrN, TiN, TiAlN coatings and nanolayered TiAlN/CrN multilayer coatings prepared by reactive direct current magnetron sputtering. Thin Solid Films. 2006;514(1–2):204–11.

46. Fontalvo GA, Daniel R, Mitterer C. Interlayer thickness influence on the tribological response of bi-layer coatings. Tribol Int [Internet]. 2010;43(1–2):108–12. Available from: http://dx.doi.org/10.1016/j.triboint.2009.05.002

47. Oliver, W.C. and Pharr G. An improved technique for determining hardness and elastic modulus using load and displacement sensing indentation experiments. J Mater Res. 1992;7(6):1564–1583.

48. Echavarría AM, Robledo S, Bejarano G. G, G. GB. Influencia de las nanopartículas de Ag sobre las propiedades mecánicas y tribológicas y en el efecto citotóxico y bactericida de los recubrimientos de TaN(Ag). Rev Metal [Internet]. 2017;53(1):85. Available from: http://revistademetalurgia.revistas.csic.es/index.php/revistademetalurgia/article/view/1399

49. Echavarría García AM, Bejarano Gaitán G, Quirama Ossa AC, Osorio Vélez JA. Deposition and properties characterization of TaN coatings deposited at different nitrogen contents. Rev EIA, Fac Ing. 2016;13:69–80.

50. Janczuk B, Chibowski E, Bruque J., Kerkeb M., F GC. On the Consistency of Surface Free Energy Components as Calculated fron Contact Angles of Different Liquids: An Application to the Cholesterol Surface. J Colloid

Interface Sci. 1993;159:421–8.

51. Oliveira R, Azeredo J, Teixeira P, Fonseca A. The role of hydrophobicity in bacterial adhesion. Bioline. 2001;11–22.

52. Żenkiewicz M. Methods for the calculation of surface free energy of solids. J Achiev Mater Manuf Enginnering. 2007;24(1):137–45.

53. Marques SM, Manninen NK, Ferdov S, Lanceros-Mendez S, Carvalho S. Ti1-xAgx electrodes deposited on polymer based sensors. Appl Surf Sci. 2014;317:490–5.

54. Musil J, Vlcek J. Magnetron sputtering of hard nanocomposite coatings and their properties. Surf Coatings Technol. 2001;557–66.

55. Mulligan CP, Gall D. CrN–Ag self-lubricating hard coatings. Surf Coatings Technol. 2005 Nov;200(5–6):1495–500.

56. Zeman P. Structure and properties of hard and superhard Zr – Cu – N nanocomposite coatings. Mater Sci Eng A. 2000;289:189–97.

57. Hsieh JH, Yeh TH, Chang SY, Li C, Tseng CC, Wu W. Mechanical and antibacterial behaviors of TaN-Cu nanocomposite thin films after multi-rejuvenation. Surf Coatings Technol. 2013;228(SUPPL.1):81–5.

58. Hanizam, Soufhwee HAR, Anuar KAR, Md. Nizam AR, Mohamad N. The effect of pulse DC and DC substrate bias during in situ cleaning PVD process on surface roughness. Procedia Eng. 2013;53:562–8.

59. Lee HS, Guo VW, Zhu JG, Laughlin DE. Control of resputtering in biased CoCrPt-SiO2 media to enhance grain decoupling and grain size distribution. J Appl Phys. 2008;103(7):23–5.

60. Garcia D, Piratoba U. (Ti,Al)N coatings on AISI 4140 by R.F Sputtering. dyna. 2007;181–5.

61. Petrov I, Barna PBB, Hultman L, Greene JEE. Microstructural evolution during film growth. J Vac Sci Technol A Vacuum, Surfaces, Film. 2003;21(5):S117.

62. Barna PB, Adamik M. Fundamental structure forming phenomena of polycrystalline films and the structure zone models. Thin Solid Films. 1998;317:27–33.

63. Pandiyaraj KN, Selvarajan V, Heeg J, Junge F, Lampka A, Barfels T, et al. Influence of bias voltage on diamond like carbon (DLC) film deposited on polyethylene terephthalate (PET) film surfaces using PECVD and its blood compatibility. Diam Relat Mater. 2010;19(7–9):1085–92.

64. Salmerón-Sánchez M, Rico P, Moratal D, Lee TT, Schwarzbauer JE, García AJ. Role of material-driven fibronectin fibrillogenesis in cell differentiation. Biomaterials. 2011;32(8):2099–105.

65. Marques SM, Rico P, Carvalho I, Gómez Ribelles JL, Fialho L, Lanceros-Méndez S, et al. MC3T3-E1 Cell Response to Ti 1– x Ag x and Ag-TiN x Electrodes Deposited on Piezoelectric Poly(vinylidene fluoride) Substrates for Sensor Applications. ACS Appl Mater Interfaces. 2016;

66. Chesmel KD, Clark CC, Brighton CT, Black J. Cellular responses to chemical and morphologic aspects of biomaterial surfaces. II. The biosynthetic and migratory response of bone cell populations. J Biomed Mater Res. 2004;29(9):1101–10.

67. Healy KE, Thomas CH, Rezania A, Kim JE, McKeown PJ, Lom B, et al. Kinetics of bone cell organization and mineralization on materials with patterned surface chemistry. Biomaterials. 1996;17(2):195–208.

68. Xu C, Yang F, Wang S, Ramakrishna S. In vitro study of human vascular endothelial cell function on materials with various surface roughness. J Biomed Mater Res - Part A. 2004;71(1):154–61.

69. Kieswetter K, Schwartz Z, Hummert T, Cochran D, Simpson J, DD D, et al. Surface roughness modulates the local production of growth factors and cytokines by osteoblast-like MG-63 cells. J Biomed Mater Res. 1996;32(1):55–63.

70. Anselme K, Bigerelle M, Noel B, Dufresne E, Judas D, Iost A, et al. Qualitative and quantitative study of human osteoblast adhesion on materials with various surface roughnesses. J Biomed Mater Res. 2000;49(2):155–66.

71. Rodriguez-Cano A, Pacha-Olivenza MA, Babiano R, Cintas P, González-Martín ML. Non-covalent derivatization of aminosilanized titanium alloy implants Silver-enhanced coating of antibacterial organics. Surf Coatings Technol. 2014;245:66–73.

72. Kirkham GR, Cartmell SH. Genes and Proteins Involved in the Regulation of Osteogenesis. In: Genes and Osteogenesis. 2007. p. 1–22.

73. Shtansky D V., Batenina I V., Kiryukhantsev-Korneev P V., Sheveyko AN, Kuptsov KA, Zhitnyak L, et al. Ag and Cu doped multifunctional bioactive nanostructured TiCaPCON films. Appl Surf Sci. 285:331–43.

74. Lee SM, Lee BS, Byun TG, Song KC. Preparation and antibacterial activity of silver-doped organic-inorganic hybrid coatings on glass substrates. Colloids Surfaces A Physicochem Eng Asp. 2010;355(1–3):167–71.

75. Sanches-Valdés S, Ramírez-vargas E, Ortega-Ortiz H, Ramos-de valle L., Méndez-Nonell J, Mondragón-Chaparro M, et al. Silver nanoparticle deposition on hydrophilic multilayer film surface and its effect on antimicrobial activity. J Appl Polym Sci. 2012;123(7):2643–50.

76. Avila-Alfaro J., Sánchez-Valdes , SL Ramos-deValle F, Ortega-Ortiz H, Méndez-Nonell J, Patiño-Soto A., Narro-Cespedes, R.I Perera-Mercado, Y.A Avalos-Belmontes F. Ultrasound Irradiation Coating of Silver Nanoparticle on ABS Sheet Surface. J Inorg Organomet Polym Mater. 2013;23:673–83.

77. Yao KS, Wang DY, Chang CY, Weng KW, Yang LY, Lee SJ, et al. Photocatalytic disinfection of phytopathogenic bacteria by dye-sensitized TiO2 thin film activated by visible light. Surf Coatings Technol. 2007;202(4–7):1329–32.

78. Rosenberg M, Rosenberg E, Judes H, Weiss E. Bacterial adherence to hydrocarbons and to surfaces in the oral cavity. FEMS Microbiol Lett. 1983;20(1):1–5.

79. Gibbons RJ, Etherden I. Comparative hydrophobicities of oral bacteria and their adherence to salivary pellicles. Infect Immun. 1983;41(3):1190–6.

80. Nesbitt WE, Doyle RJ, Taylor KG. Hydrophobic Interactions and the Adherence of Streptococcus sanguis to Hydroxylapatite. Infect Immun. 1982;38(2):637–44.

81. Van Pelt A, Weerkamp A, Uyen M, Busscher H, Jong H, Arends J. Adhesion of Streptococcus sanguis CH3 to Polymers with Different Surface Free Energies. Appl Environ Microbiol. 1985;49(5):1270–5.

82. Gibbons RJ, L C, Hay D. Strain of Streptococcus mutans and Streptococcus sobrinus attach to differnts pelicle receptors. Infect Inmum. 1986;55:555–61.

83. Liu T, Liao H, Lin C, Hu S, Chen S. Biofunctional ZnO Nanorod Arrays Grown on Flexible Substrates. Langmuir. 2006;12(24):5804–9.

84. Ábalos C. Adhesión bacteriana a biomateriales. Av Odontoestomatol. 2005 Feb;21(1):347–53.

85. An YH, Friedman RJ. Concise review of mechanisms of bacterial adhesion to biomaterial surfaces. J Biomed Mater Res. 1998;43(3):338–48.

86. Yuranova T, Rincon AG, Bozzi A, Parra S, Pulgarin C, Albers P, et al. Antibacterial textiles prepared by RF-plasma and vacuum-UV mediated deposition of silver. 2003;161:27–34.

87. Feng QL, Wu J, Chen GQ, Cui FZ, Kim TN, Kim JO. A mechanistic study of the antibacterial effect of silver ions on Escherichia coli and Staphylococcus aureus. J Biomed Mater Res. 2000;52(4):662–8.

88. Klasen HJ. Historical review of the use of silver in the treatment of burns . I . Early uses. 2000;26.

89. Sondi I, Salopek-Sondi B. Silver nanoparticles as antimicrobial agent: a case study on E. coli as a model for Gram-negative bacteria. J Colloid Interface Sci. 2004 Jul 1;275(1):177–82.

90. Panacek A, Kolar M, Vecerova R, Prucek R, Soukupová J, Krystof V, et al. Antifungal activity of silver nanoparticles against Candida spp. Biomaterials. 2009;30(31):6333–40.

91. Li L, Sun J, Li X, Zhang Y, Wang Z, Wang C, et al. Controllable synthesis of monodispersed silver nanoparticles as standards for quantitative assessment of their cytotoxicity. Biomaterials. 2012;33(6):1714–21.

92. Gopinath P, Gogoi SK, Chattopadhyay A, Ghosh SS. Implications of silver nanoparticle induced cell apoptosis for in vitro gene therapy. Nanotechnology. 2008;19(7):75104.

93. Borm P. Research Strategies for Safety Evaluation of Nanomaterials, Part V: Role of Dissolution in Biological Fate and Effects of Nanoscale Particles. Toxicol Sci. 2005;90(1):23–32.